

## ON ESTIMATING THE MASS OF KEPLERIAN ACCRETION DISKS IN H<sub>2</sub>O MASER GALAXIES

C. Y. KUO<sup>1</sup>, M. J. REID<sup>2</sup>, J. A. BRAATZ<sup>3</sup>, F. GAO<sup>3</sup>, C. M. V. IMPELLIZZERI<sup>3,4</sup>, W. T. CHIEN<sup>1</sup>

<sup>1</sup>Physics Department, National Sun Yat-Sen University, No. 70, Lien-Hai Rd, Kaosiung City 80424, Taiwan, R.O.C

<sup>2</sup>Harvard-Smithsonian Center for Astrophysics, 60 Garden Street, Cambridge, MA 02138, USA

<sup>3</sup>National Radio Astronomy Observatory, 520 Edgemont Road, Charlottesville, VA 22903, USA and

<sup>4</sup>Joint ALMA Office, Alonso de Crdova 3107, Vitacura, Santiago, Chile

*Draft version August 13, 2018*

### ABSTRACT

H<sub>2</sub>O maser disks with Keplerian rotation in active galactic nuclei offer a clean way to determine accurate black hole mass and the Hubble constant. An important assumption made in using a Keplerian H<sub>2</sub>O maser disk for measuring the black hole mass and the Hubble constant is that the disk mass is negligible compared to the black hole mass. To test this assumption, a simple and useful model can be found in Huré et al. (2011). In this work, the authors apply a linear disk model to a position-dynamical mass diagram and re-analyze position-velocity data from H<sub>2</sub>O maser disks associated with active galactic nuclei. They claim that a maser disk with nearly perfect Keplerian rotation could have disk mass comparable to the black hole mass. This would imply that ignoring the effects of disk self-gravity can lead to large systematic errors in the measurement of black hole mass and the Hubble constant. We examine their methods and find that their large estimated disk masses of Keplerian disks are likely the result of their use of projected instead of 3-dimensional position and velocity information. To place better constraints on the disk masses of Keplerian maser systems, we incorporate disk self-gravity into a 3-dimensional Bayesian modelling program for maser disks and also evaluate constraints based on the physical conditions for disks which support water maser emission. We find that there is little evidence that disk masses are dynamically important at the  $\lesssim 1\%$  level compared to the black holes.

*Subject headings:* accretion, accretion disks – galaxies: nuclei – galaxies: masers – galaxies: active – galaxies: ISM – galaxies: Seyfert

### 1. INTRODUCTION

H<sub>2</sub>O megamasers from circumnuclear disks (megamaser disks) in active galaxies provide a unique way to probe active galactic nuclei. Megamaser disks, such as in the archetypal maser galaxy NGC 4258 (e.g. Herrnstein et al. 1999), are typically smaller ( $r \sim 0.2$  pc in NGC 4258) than the gravitational sphere of influence of their supermassive black holes (BHs;  $r \sim 1$  pc in NGC 4258). This guarantees that the gravitational potential is dominated by the central point mass. As a result, the rotation curves of megamasers disks often follow a nearly perfect Keplerian law, with velocity falling as the inverse square root of radius, allowing one to easily determine the masses of supermassive BHs ( $M_{\text{BH}}$ ) to a few percent-level accuracy (e.g. Kuo et al. 2011; Gao et al. 2016).

In addition to BH mass measurement, the Keplerian rotation of a megamaser disk also allows one to use the orbits of the masing gas as a standard ruler and determine an angular-diameter distance to a galaxy. This forms the basis of the Megamaser Cosmology Project (MCP; e.g. Braatz et al. 2010) for which one attempts to make precise determinations of the Hubble constant ( $H_0$ ) by modeling the geometrical and kinematic information of the megamaser disks (e.g. Reid et al. 2013; Kuo et al. 2013; Kuo et al. 2015; Gao et al. 2016).

While many megamaser disks display nearly perfect Keplerian rotation curves, slight deviations from Keplerian rotation have been reported in the literature. For NGC 4258, Herrnstein et al. (2005) show that the projected rotation curve of high-velocity masers displays a

$\sim 9$  km s<sup>-1</sup>, or 0.8%, flattening of the line-of-sight velocities with respect to Keplerian motion. Careful modeling of this slight deviation can provide a constraint on the mass and accretion rate of the disk (e.g. Herrnstein et al. 2005), allowing one to obtain important physical properties for exploring AGN.

Constraining the total mass of the maser disk ( $M_{\text{D}}$ ) can have important implications. An upper limit on  $M_{\text{D}}$  is important for understand the warping mechanism of a disk (e.g. Caproni et al. 2007, Martin 2008, Ulubay-Siddiki, Gerhard, & Arnaboldi 2009, Bregman & Alexander 2012). Except for a few cases, such as NGC 1068 (Lodato & Bertin 2003) for which  $M_{\text{D}}$  is known to be comparable to  $M_{\text{BH}}$ , all previous measurements of  $M_{\text{BH}}$  and  $H_0$  from megamaser disks with nearly perfect Keplerian rotation curves assume that  $M_{\text{D}}$  is negligible in comparison with  $M_{\text{BH}}$ . Based on this assumption, measurements of  $M_{\text{BH}}$  and  $H_0$  with at few percent level accuracy can be achieved when the data quality is high, and the measurement uncertainty is dominated by measurement error. While  $M_{\text{D}} \ll M_{\text{BH}}$  seems to be a good assumption for a nearly perfect Keplerian disk, the analysis performed by Huré et al. (2011) challenges this assumption.

Based on a theoretical model of accretion disks by Huré et al. (2008), Huré et al. (2011) derive an expression for the dynamical mass of orbiting gas in a megamaser disk as a function of  $M_{\text{D}}$ ,  $M_{\text{BH}}$ , and a surface density profile. These authors show that  $M_{\text{D}}$  and  $M_{\text{BH}}$  for a megamaser disk system can be inferred from a *position-dynamical mass* diagram. Their most striking result from apply-

ing this technique to seven published megamaser systems is that the claimed disk mass ( $M_D = 6.2 \times 10^6 M_\odot$ ) for UGC 3789, which is comparable to their estimated BH mass ( $M_{BH} = 8.1 \times 10^6 M_\odot$ ). This result is quite puzzling because it contradicts the general picture that Keplerian rotation implies the concentration of the gravitating mass at the dynamical center of an orbit. Furthermore, were the analysis of Huré et al. (2011) to be correct, it would suggest that systematic errors in BH mass and the Hubble constant from applying the H<sub>2</sub>O megamaser technique to Keplerian maser systems could be significantly underestimated.

In order to better understand why Huré’s estimated disk masses in Keplerian maser disks could be so large, we re-examine their analysis in Section 2. In Section 3, we estimate the masses of megamaser disks more precisely by incorporating the accretion disk model adopted by Huré et al. (2011) in the 3-dimensional disk modelling code used by the MCP. This allows us to evaluate the magnitude of systematic errors in the BH mass from ignoring disk self-gravity. In Section 4, we discuss the implications of our results and make conclusions.

## 2. RE-EXAMINATION OF THE POSITION–DYNAMICAL MASS DIAGRAM

A position–dynamical mass (PDM) diagram can indicate the enclosed gravitating mass as a function radius in an accretion disk. As shown in Huré et al. (2011), the dynamical mass  $\mu$  for a maser disk system can be defined as

$$\mu = \frac{rv^2}{G} \equiv \mu(\bar{w}), \quad (1)$$

where  $r$  is the physical radius of a masing spot in a circular orbit of the disk,  $v$  is the orbital velocity of the masing spot, and  $\bar{w}$  is the normalized radius of the masing gas. The normalized radius is defined as  $\bar{w} = r/a_{\text{out}}$ , where  $a_{\text{out}}$  is the outer radius of a maser disk.

Huré et al. (2011) analyze the position–dynamical mass diagrams for seven megamaser disks published before 2011 (i.e. IC 1481, UGC 3789, NGC 3393, NGC 4258, NGC 1068, NGC 4945, and Circinus). They find that, in most of these systems, the masses of the accretion disks are comparable to (i.e. UGC 3789, NGC 1068), or substantially greater (i.e. IC 1481, NGC 3393, Circinus) than, the central BH masses of  $\sim 10^7 M_\odot$ . For the archetypal maser galaxy, NGC 4258, while their estimated disk mass is substantially smaller than the BH mass, the best-fit disk mass is  $\sim 10^6 M_\odot$ , which may be large enough to contribute to uncertainty in the distance determination for this galaxy using the H<sub>2</sub>O megamaser technique (Herrnstein et al. 1999, Humphreys et al. 2013), and hence could affect the accuracy of Hubble constant determination based on the NGC 4258 distance (e.g. Riess et al. 2016).

To explore why Huré’s analysis allows massive disks in UGC 3789 and NGC 4258, we wanted to reproduce their analysis, but could not since their position–velocity data points were “obtained by digitalizing graphs when published ...”. This is unfortunate, since the measurements of maser position and velocity for these two galaxies were

available online in electronic form<sup>12</sup>. Furthermore, the authors did not publish their digitized data, making it impossible to repeat their analysis. So, in order to better understand the origin of their large disk masses, we first repeated the model-fitting done by Huré et al. (2011) using the measurements of maser position and velocity from data in the original papers.

### 2.1. The Maser Systems for the New Analysis

In our analysis using the PDM diagram for estimating the disk mass, we will focus on the six published Keplerian maser systems (UGC 3789, NGC 6323, NGC 6264, MRK 1419, NGC 5765b, and NGC 4258) which are the primary targets for accurate  $H_0$  or geometric distance measurements based on the H<sub>2</sub>O megamaser technique (Reid et al. 2013). Our main goal is to examine whether the basic assumption that disk mass is negligible compared to the BH mass in *Keplerian maser disks* holds when using the megamaser technique to measure BH mass and Hubble constant. Whether or not non-Keplerian disks<sup>3</sup> have substantial disk masses is not the focus of this paper. Among these six systems we examine here, UGC 3789 and NGC 4258 allow a direct comparison between our work and that of Huré et al. (2011).

We do not include the five maser systems, IC 1481, NGC 3393, NGC 1068, NGC 4945, and Circinus – in Huré et al. (2011) because these systems either have complicated maser distributions, kinematics deviating significantly from Keplerian rotation, or the uncertainties of the maser position measurements are relatively large. While these factors may not prevent BH mass estimates with accuracy sufficient for understanding the  $M_{BH} - \sigma_*$  relation (e.g. Ferrarese & Merritt 2000; Gebhardt et al. 2000; Gütekin et al. 2009; Greene et al. 2016), which is a relation in a log-log plot, these factors make these systems non-ideal for accurate  $H_0$  determination because the systematic uncertainties resulting from these factors could make the  $H_0$  determination with percentage-level accuracy difficult, especially if non-gravitation effects such as outflows are involved (e.g. Greenhill et al. 2003). Therefore, whether these systems have substantial disk masses are cosmologically less important.

Moreover, these factors, plus the lack of centripetal acceleration measurements of maser features in these systems which constrain maser positions along the line-of-sight in the disks, prevent us to perform the more robust 3-dimensional modeling of the disk shown in section 3 for determining the disk masses in these systems. We thus ignore them in our analysis.

### 2.2. The Basic Disk Model

The disk model derived by Huré et al. (2011) for describing the dynamical mass distribution of an accretion disk involves a complicated, non-linear equation that involves the BH mass ( $M_{BH}$ ), disk mass ( $M_D$ ), inner/outer

<sup>1</sup> see Table 5 in <http://iopscience.iop.org/article/10.1086/512718/fulltext/> for NGC 4258

<sup>2</sup> see Table 2,3,4 in <http://iopscience.iop.org/article/10.1088/0004-637X/695/1/287/meta> for UGC 3789

<sup>3</sup> In our analysis, a non-Keplerian disk is defined as a maser disk system in which the reduced  $\chi^2$  of the rotation-curve fitting with the Keplerian rotation law is greater than 1.5.

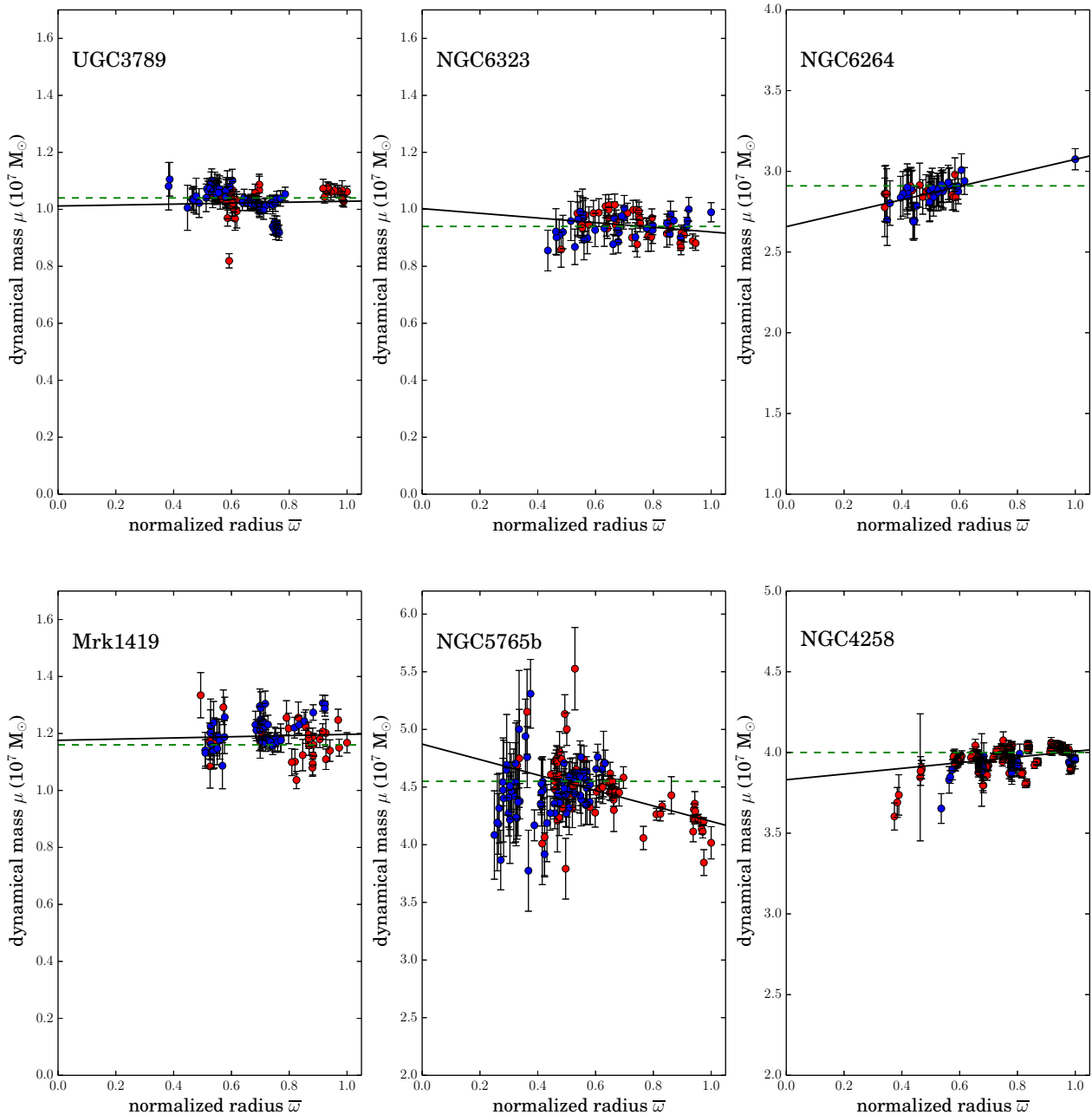


FIG. 1.— The position–dynamical mass diagrams for six disk maser systems that display nearly perfect Keplerian rotation curves. The red and blue dots show the redshifted and blueshifted maser spots in a disk, respectively. In each plot, the black line shows the best linear fit to the data, and green dashed line shows black hole mass obtained from fitting the Keplerian rotation law to the observed rotation curve for each maser system (Kuo et al. 2011; Gao et al. 2016; Humphreys et al. 2013). The slope of the black line represents the mass of the disk in the context of the Huré model while its intercept with the vertical axis of the plot indicates the black hole mass of the system.

radius of the accretion disk, and the surface density distribution of the disk (see equation (6) in Huré et al. 2011). They simplify this equation by assuming standard parameters of astrophysical disks, which lead to a linear equation for the dynamical mass distribution:

$$\mu(\bar{r}) = M_{\text{BH}} + M_{\text{D}}\bar{r} . \quad (2)$$

This shows that the observational data plotted in a PDM diagram should display a dynamical mass which is a linear function of the normalized radius. By fitting a straight line to the distribution, the slope gives  $M_{\text{D}}$  and the intercept gives  $M_{\text{BH}}$ . We refer to Equation (2) as the

“linear model.”

### 2.3. Evaluating the Dynamical Mass

Before one can fit Equation (2) to the data, one has to first compute the dynamical mass  $\mu(\bar{r})$  with the observed maser positions and velocities by using Equation (1). To obtain the physical radii of maser spots, we define the position of the dynamical center of the system on the plane of the sky ( $x_0, y_0$ ) by adopting the published values from 3-dimensional disk modelling (see the reference papers shown in Table 1). When dealing with maser position uncertainties, rather than using formal

TABLE 1  
RESULTS OF LINEAR-FITTING IN THE POSITION– DYNAMICAL MASS DIAGRAMS

| Galaxy Name | Distance (Mpc) | N   | $M_{\text{BH}}$ ( $10^7 M_{\odot}$ ) | $M_{\text{D}}$ ( $10^7 M_{\odot}$ ) | $\chi^2_{\nu}$ | $\sigma_{\mu}$ ( $10^7 M_{\odot}$ ) | Reference Paper              |
|-------------|----------------|-----|--------------------------------------|-------------------------------------|----------------|-------------------------------------|------------------------------|
| UGC 3789    | 46.4           | 113 | $1.01 \pm 0.04$                      | $0.02 \pm 0.05$                     | 3.04           | 0.05                                | Reid et al. (2013)           |
| NGC 6323    | 106.7          | 76  | $1.00 \pm 0.03$                      | $-0.08 \pm 0.04$                    | 1.10           | 0.04                                | Kuo et al. (2015)            |
| NGC 6264    | 139.4          | 55  | $2.66 \pm 0.02$                      | $0.42 \pm 0.03$                     | 0.24           | 0.05                                | Kuo et al. (2013)            |
| MRK 1419    | 72.2           | 76  | $1.18 \pm 0.08$                      | $0.02 \pm 0.09$                     | 2.34           | 0.06                                | Impellizzeri et al. in prep. |
| NGC 5765b   | 126.3          | 152 | $4.87 \pm 0.06$                      | $-0.70 \pm 0.07$                    | 2.19           | 0.25                                | Gao et al. (2016)            |
| NGC 4258    | 7.6            | 183 | $3.83 \pm 0.06$                      | $0.18 \pm 0.06$                     | 4.56           | 0.06                                | Humphreys et al. (2013)      |

NOTE. — Column (1): Name of the galaxy; column (2): galaxy distance adopted in the calculation of dynamical mass; column (3): number of data points for fitting; columns (4) and (5): the best-fit black hole and disk masses, with their uncertainties inflated by the square-root of the reduced  $\chi^2$ ; column (6): the reduced  $\chi^2$  of the fitting; column (7): the dispersion of the dynamical mass with respect to the linear model; column (8): references for the positions and velocities of maser spots.

fitting uncertainties from images, which tend to be optimistic for high signal-to-noise data, we include more realistic “error floors” adopted in the reference papers to account for the systematic uncertainties. To obtain orbital velocity data, we subtract the recession velocity of the galaxy from the observed maser velocities. For NGC 4258 we also correct for effects of inclination of the maser disk, which shows a  $\approx 8^\circ$  warping. No disk inclination corrected are needed for the other five systems, because those disks are within  $\approx 1^\circ$  of being exactly edge-on.

#### 2.4. Fitting Results

Figure 1 shows the PDM diagrams for the six systems discussed here. The red and blue dots represent the redshifted and blueshifted “high-velocity” maser spots, respectively. The solid black lines show the best linear fits to the data, and green dashed line shows black hole mass obtained from the original disk fitting, which assumed pure Keplerian rotation (Kuo et al. 2011; Gao et al. 2016; Humphreys et al. 2013). These results are summarized in Table 1. In order to make a direct comparison with Huré et al. (2011), we first focus on UGC 3789 and NGC 4258.

For UGC 3789, one can see dramatic differences between the inferred disk mass from our Figure 1 and the Huré et al. (2011) Figure 1. We note that Huré used only one-third of the available position–velocity data. Using the full data set, we do not see a significant slope in the PDM diagram. The best-fit  $M_{\text{D}} = (0.02 \pm 0.05) \times 10^7 M_{\odot}$  is consistent with zero disk mass. In contrast, Huré et al. (2011) derive a disk mass of  $M_{\text{D}} \sim 0.62 \times 10^7 M_{\odot}$ , which is comparable to their best-fit BH mass ( $M_{\text{BH}} \sim 0.81 \times 10^7 M_{\odot}$ ). The significant difference between these two results suggest that the large estimated disk mass for UGC 3789 from Huré et al. (2011) is likely caused by errors from reading data values from graphs by eye and excluding the majority of the measured data.

For NGC 4258, there is marginal evidence for a slope in the PDM diagram. Our best-fit  $M_{\text{D}} (0.18 \pm 0.06 \times 10^7 M_{\odot})$  is consistent with the values from Huré et al. ( $\sim 0.16 \times 10^7 M_{\odot}$ ), and the BH mass differs only by 5% between these two analysis. The disk mass is formally non-zero only at the  $3\sigma$  level, and there may be some outlying data that contribute to this result. So, before concluding that there might be a measurable disk mass in NGC 4258, it is instructive to examine the PDM diagrams for the other four Keplerian rotating systems.

From Figure 1, one can see that Mrk 1419 does not have a significant slope in the PDM diagram, and this leads to a negligible disk mass  $M_{\text{D}} = (0.02 \pm 0.09) \times 10^7 M_{\odot}$ . NGC 6264 shows the most formally significant slope among the six systems presented here, and the corresponding disk mass is  $M_{\text{D}} = (0.42 \pm 0.03) \times 10^7 M_{\odot}$ . On the other hand, both NGC 6323 and NGC 5765b show negative slopes in the PDM diagrams, implying *negative* disk masses: ( $M_{\text{D}} = (-0.08 \pm 0.04) \times 10^7 M_{\odot}$  for NGC 6323 and  $M_{\text{D}} = (-0.70 \pm 0.07) \times 10^7 M_{\odot}$  for NGC 5765b). Note that both NGC 6323 and NGC 5765b have very well-ordered maser disks, which do not appear to have complicated spatial structures (see Kuo et al. 2015; Gao et al. 2016), and their maser kinematics can be well-fitted by Keplerian rotation. Therefore, the negative disk masses derived from the PDM diagrams for these two galaxies, especially for NGC 5765b, are most likely not results from fitting maser disks with features that cannot be well-modelled (e.g. disk thickness) or features that are suggestive more complicated physics (e.g. outflows in Circinus; Greenhill et al. 2003). If so, what else can cause negative, non-physical disk mass estimates?

#### 2.5. The Origin of the Scatter in Dynamical Mass Estimates

In the sixth column in Table 1, one can see that four of the six maser disk systems here have reduced  $\chi^2_{\nu}$  values greater than two, which implies either that the linear model described by Equation (2) does not well fit the data or that the uncertainties in the measurements are underestimated. For UGC 3789, NGC 5765b, and NGC 4258, one can see that some groups of maser spots systematically lie either above or below the linear model. This could be caused by “astrophysical noise,” indicating that not all maser spots perfectly reflect an idealized thin disk. With the degree and distribution of scatter seen in these plots, it is not unreasonable that negative disk mass estimates can appear in certain cases. For example, while the present fit for UGC 3789 shows negligible slope, were one to ignore the group of redshifted masers at the outer most radii, one would obtain a small but statistically significant negative slope owing mostly to the clump of blue shifted spots below the fitted line near a normalized radius of 0.75.

Based on our experience modeling maser disks (e.g. Kuo et al. 2013; Reid et al. 2013), we argue that some of the scatter seen in the PDM diagrams most likely orig-

inates from the differences between the projected and 3-dimensional maser velocities and radii. When estimating dynamical masses of maser disks using Equation (2), the Huré et al. analysis assumes that the observed velocities and radii of high-velocity masers are identical to their full 3-dimensional orbital values. Note that these assumptions are valid only if the high-velocity masers lie exactly on the mid-line of the disk (i.e. the intersection between the disk plane and plane of the sky). In reality, the high-velocity masers in a maser disk can lie in a region that deviates from the mid-line of the disk by  $\sim 10\text{--}20^\circ$  (e.g. Kuo et al. 2011, Reid et al. 2013, Gao et al. 2016). Because of this, the observed projected velocities of the outermost redshifted masers in NGC 5765b are substantially smaller than their true orbital velocities. This leads to a smaller apparent dynamical mass at large radii, which would result in a negative disk mass based on PDM fitting.

While we speculate that ignoring deviations of maser positions from the mid-line of the disk could be the primary cause of a negative disk mass, it is also conceivable that gas and radiation pressure in the radial direction of the disk could also lead to a negative slope in a PDM diagram. This is because these pressures can provide support against gravity from the BH, making the orbital velocity smaller than the Keplerian value at a given radius and the dynamical mass will appear to be smaller than the true value. If the dynamical mass estimate that includes the pressure effect happens to decrease with radius, a negative slope in the PDM diagram will result. However, as we will show in detail in section 3.5, while radiation and gas pressure can indeed introduce a negative slope in a PDM diagram, their effect on the dynamical mass estimate is too small to explain the scatter seen in Figure 1. Therefore, we can exclude the possibility that negative disk masses can result from thermal or radiation pressure for the maser disks discussed in this paper.

We conclude that while the disk model proposed by Huré et al. (2011) can provide a simple way to determine the BH mass and disk mass, the PDM diagram is not a robust tool to derive accurate  $M_{\text{BH}}$  and  $M_{\text{D}}$ , because astrophysical noise and the use of projected radii and velocities (instead of 3-dimensional values) can bias such dynamical mass estimates.

### 3. DERIVING DISK MASS FROM 3-DIMENSIONAL MODELING

A promising way to avoid bias when estimating  $M_{\text{BH}}$  and  $M_{\text{D}}$  is to incorporate the linear model of Huré et al. into the 3-dimensional modeling code used by the Megamaser Cosmology Project (e.g. Humphreys et al. 2013). This removes projection biases and reduces systematic errors caused by ignoring warped disk structures. Before formally showing the results of  $M_{\text{BH}}$  and  $M_{\text{D}}$  measurements using the 3-dimensional model, it is helpful to first discuss the model fitting assuming zero disk mass. This will serve as the basis for comparisons, in order to see how much  $M_{\text{BH}}$  can change when  $M_{\text{D}}$  is included in the analysis. In the following, we will call the model in which  $M_{\text{D}}$  is ignored the “fiducial” model.

#### 3.1. The Fiducial Model

The fiducial model described here was first introduced in Reid et al. (2013) to determine accurate  $H_0$  using the

maser disk in UGC 3789. The disk model is described by 15 global parameters including the  $H_0$ ,  $M_{\text{BH}}$ , sky position of the dynamical center of a maser disk, the recession velocity of the galaxy, and parameters that described the warped structure and the eccentricity of the maser orbits (see Reid et al. 2013 and Humphreys et al. 2013 for details). The galaxy distance is calculated from  $H_0$  and recession velocity parameters in the fitting program.

The model assumes that the maser spots orbit around a BH with Keplerian rotation law, and the relationship between the maser velocity  $v_{\text{orb}}$  and the BH mass can be described by

$$v_{\text{orb}} = \sqrt{\frac{GM_{\text{BH}}}{r}}, \quad (3)$$

where  $r$  is the orbital radius of a particular maser spot. The data that are fitted with the fiducial model are positions, velocities, and accelerations of the maser spots in a disk. Among these data, maser accelerations play a crucial role for constraining the spatial location of a maser spot along the line-of-sight.

For the purpose of estimating  $M_{\text{D}}$  relative to  $M_{\text{BH}}$  in the context of the Huré et al. (2011) approach, we held  $H_0$  constant at a value consistent with the assumed angular–diameter distance (listed in Table 1) and recession velocity for each galaxy. The program uses a Markov chain Monte Carlo (McMC) approach, and we adopted the median of the marginalized posterior density functions as best-fit parameter values, with the uncertainties spanning 68% confidence intervals. We usually generated  $\geq 10^9$  McMC trials in order to ensure convergence of the Bayesian fitting. The results of applying the fiducial model to fit the data are summarized in Table 2.

#### 3.2. Results from Including the Disk Model

Implementing the disk model of Huré et al. in our 3-dimensional disk modeling code is straightforward. Based on Equation (1), one can express the orbital velocity of a maser spot as a function of the dynamical mass and orbital radius as

$$v_{\text{orb}} = \sqrt{\frac{G(M_{\text{BH}} + M_{\text{D}}\bar{w})}{r}}. \quad (4)$$

Note that this equation is essentially equivalent to Equation (3) if one replaces  $M_{\text{BH}}$  in the equation with the dynamical mass defined by Equation (2). Here,  $M_{\text{D}}$  is added in the disk model as a new global parameter.

Figures 2 & 3 show the marginalized PDFs of  $M_{\text{BH}}$  and  $M_{\text{D}}$  for the six maser systems considered here. The dashed lines represent the PDFs of  $M_{\text{BH}}$  derived using the fiducial model, and the dotted lines show the PDFs for  $M_{\text{BH}}$  and  $M_{\text{D}}$  using the linear model, which allows for disk mass. Table 2 summarizes the best-fit values for  $M_{\text{BH}}$  and  $M_{\text{D}}$ . The reduced  $\chi^2_{\nu}$  of the fits now range from  $\approx 0.5 - 1.4$  (see column 11 in Table 2), indicating considerable improvement over those in Table 1 where projected, instead of 3-dimensional, velocities and radii were used. These figures reveal that disk masses range from about  $10^5$  to  $10^6 M_{\odot}$ , and that most of these estimates are not statistically significant. In all cases, the disk masses are at least 10 times smaller than the BH masses. We conclude that there is no evidence for disk

masses comparable to BH masses as suggested by Huré et al. (2011).

### 3.3. Imposing Physical Conditions for Maser Emission

In a model that can describe H<sub>2</sub>O maser disk satisfactorily, an important condition that has to be satisfied is that the density of molecular gas,  $n_{\text{H}_2}$ , in the disk should be given by  $n_{\text{H}_2} = \sim 10^8 - 10^{10} \text{ cm}^{-3}$  in order to allow sufficient amplification and avoid thermalization of the population inversion (Herrnstein et al. 2005; Gray et al. 2016). Using the surface density profile  $\Sigma = \Sigma(r)$  adopted by Huré et al. (2011) and the fitted disk mass from the previous section, one can infer  $n_{\text{H}_2}$  at the inner edge of a maser disk by using the equation

$$n_{\text{H}_2} = \frac{\Sigma(r)}{\sqrt{2\pi} m_{\text{H}_2} H(r)}, \quad (5)$$

where  $m_{\text{H}_2}$  is the mass of the molecular hydrogen, and  $H(r)$  is the scale height of the disk as a function of radius  $r$ . Here,  $\Sigma(r) = \Sigma_{\text{out}}(r/a_{\text{out}})^{-1}$ , where  $a_{\text{out}}$  and  $\Sigma_{\text{out}}$  are radius and surface density at the outer edge of a maser disk, and  $\Sigma_{\text{out}} = M_{\text{D}}/(2\pi a_{\text{out}}^2)$ .<sup>4</sup>  $H(r)$  can be estimated from the following equation (Neufeld & Maloney 1995):

$$H(r) = c_s r \sqrt{r/GM_{\text{BH}}}, \quad (6)$$

where  $c_s$  is the sound speed of the gas in the disk; we adopt  $c_s = 2.15 \pm 0.15 \text{ km s}^{-1}$ , corresponding to a gas temperature of  $700 \pm 100 \text{ K}$  in the disk modeling. We choose  $100 \text{ K}$  as the uncertainty for gas temperature because the  $3\sigma$  uncertainty of the chosen temperature distribution corresponds to the preferred temperature range for  $22 \text{ GHz}$  H<sub>2</sub>O maser emission of  $400 - 1000 \text{ K}$  estimated by Herrnstein et al. (2005). Note that the three dimensional disk modeling presented here is insensitive to the  $100 \text{ K}$  temperature uncertainty. Increasing the uncertainty by a factor of 2 would only lead to a negligible change in BH mass and a change in the disk mass less than  $\sim 10\%$ .

In columns (9) of Table 2, we show the inferred number densities at the inner edge of the six maser disks. One can see that, except for NGC 5765b, these values (including the ranges allowed by the uncertainties) are in general substantially greater than the range for maser emission. In the case of MRK 1419 and NGC 4258,  $n_{\text{H}_2} > 10^{11} \text{ cm}^{-3}$ , for which collisions would thermalize the level populations and quench any masing. This suggests that the true upper bound for the disk mass must be smaller than the values we show in the previous section.

In order to place a more physically realistic constraint on disk mass, in our disk modeling we impose  $10^8 < n_{\text{H}_2} < 10^{10} \text{ cm}^{-3}$  between the observed inner and outer edge of a maser disk. In Figures 2 and 3, the solid black lines shows the PDFs of  $M_{\text{BH}}$  and  $M_{\text{D}}$  after imposing this density condition in the linear model, and the results of the fitting are summarized in the third row for each

<sup>4</sup> Note that this expression for  $\Sigma_{\text{out}}$  is valid only when  $a_{\text{out}} \gg a_{\text{in}}$ , where  $a_{\text{in}}$  is the radius of the inner edge of an accretion disk and is assumed to be a few Schwarzschild radii ( $R_s$ ) in Huré et al. (2011). This suggests that the disk mass discussed in Huré et al. does not only account for the mass contribution from the masing region of the disk, but also mass contribution from regions well within the inner edge of a maser disk, which typically has an inner radius of  $\sim 10^5 R_s$  (Kuo et al. 2011).

galaxy in Table 2. This considerably reduces the disk mass estimates. In this new fitting, most disk masses are all below  $10^5 M_{\odot}$ . The fractional changes in BH mass with respect to the fiducial model are 0.0%, 0.8%, 2.3%, 0.4%, 0.6%, and 0.05% for UGC 3789, NGC 6323, NGC 6264, MRK 1419, NGC 5765b, and NGC 4258, respectively. Since these uncertainties are in general smaller than the measurement errors for these galaxies, this implies that when a more realistic model for maser disks is considered, the impact of the self-gravity of the disk in the modeling is negligible for these systems.

### 3.4. Comparison with the Herrnstein Disk Model

In the previous section, we saw that the linear model gave negligible disk masses when imposing the density condition for maser emission in the disk fitting. It would be interesting to see whether different accretion disk models give similar results.

The disk model we use here for comparison was used by Herrnstein et al. (2005) to describe the maser disk in NGC 4258. In this model, which assumes steady-state accretion, the mid-plane density of the accretion disk  $\rho_{\text{mid}}$  follows the equation:

$$\rho_{\text{mid}}(r) = \frac{GM_{\text{BH}}\dot{M}}{3\pi(2\pi)^{1/2}\alpha r^3 c_s^3}, \quad (7)$$

where  $\dot{M}$  is the mass accretion rate,  $\alpha$  is the Shakura-Sunyaev viscosity parameter (Shakura & Sunyaev 1973),  $r$  is radius, and  $c_s$  is the sound speed. Given the disk scale height described by  $H = c_s r (r/GM_{\text{BH}})^{1/2}$ , one can show that the surface density profile  $\Sigma$  is proportional to  $r^{-3/2}$ , which differs from that adopted for the linear model (i.e.  $\Sigma \propto r^{-1}$ ) in Huré et al. (2011).

Using Equation (5), Herrnstein et al. (2005) derive the mass distribution  $M_{\text{D}}(r)$  in the disk :

$$M_{\text{D}}(r) = 8.3 \times 10^4 \frac{\dot{M}}{\alpha} \frac{M_{\text{BH}}^{1/2} (r^{1/2} - r_{\text{min}}^{1/2})}{c_s^2} M_{\odot}, \quad (8)$$

where  $r_{\text{min}}$  is the physical radius of the innermost maser spot in the disk.

To implement disk mass in the 3-dimensional Bayesian modeling code, we follow the approach from Herrnstein et al. (2005) and replace  $M_{\text{BH}}$  in Equation (3) by  $M_{\text{BH}} + M_{\text{D}}(r)$  :

$$v_{\text{orb}} = \sqrt{\frac{G[M_{\text{BH}} + M_{\text{D}}(r)]}{r}}. \quad (9)$$

Here,  $c_s$  in Equation (8) is added in the model with a Gaussian prior of  $2.15 \pm 0.15 \text{ km s}^{-1}$ . We also require  $n_{\text{H}_2}$  to be within  $10^8 - 10^{10} \text{ cm}^{-3}$  in the disk modelling.

Figures 4 & 5 shows the PDFs for  $M_{\text{BH}}$ ,  $\dot{M}$ , and  $M_{\text{D}}$  for the six Keplerian maser disks and the fitting results are summarized in the fourth and fifth rows for each galaxy in Table 2. Similar to Figures 2 & 3, dashed lines in the figures show the BH mass measurements based on the fiducial model. The solid and dotted lines represent measurements from the Herrnstein model with and without including constraints on gas density in the model fitting, respectively. These figures show that in all cases, the disk mass is  $\lesssim 1\%$  of the BH mass, and the fractional changes in BH mass estimates also are all  $\lesssim 1\%$ . These results

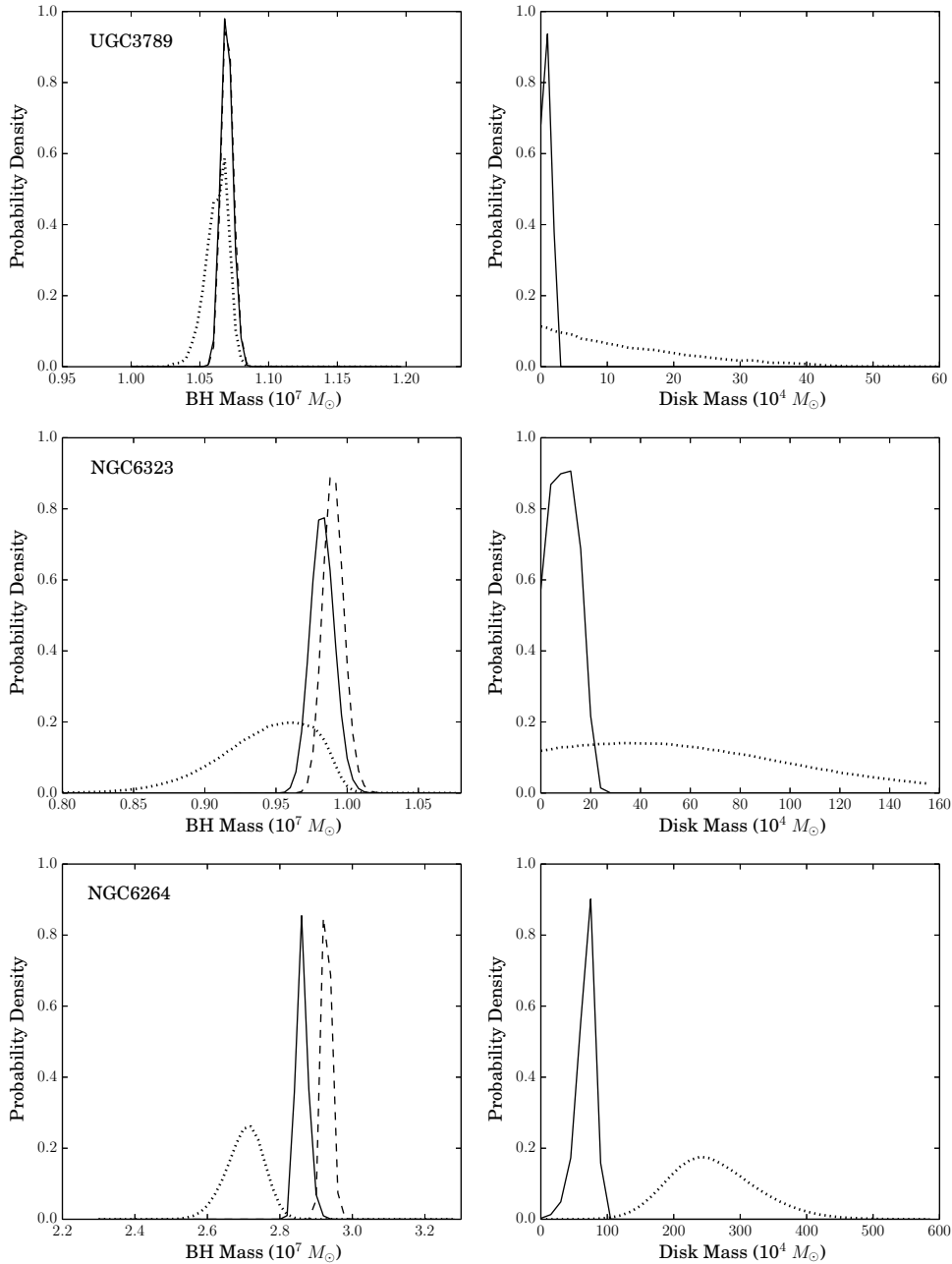


FIG. 2.— The posterior probability distribution functions (PDF) of the black hole mass and disk mass from the 3-dimensional disk modelling based on the Huré model for the Keplerian maser disks in UGC 3789, NGC 6323, and NGC 6264. The dashed lines shown in the left panels represent the PDFs of  $M_{\text{BH}}$  derived from the fiducial model in which the disk mass is assumed to be zero. The dotted and solid lines in the left and right panels show the fitting results from the linear model which either including (the solid line) or ignoring (the dotted line) the physical conditions for maser emission in the model fitting.

are consistent with  $M_{\text{D}}$  estimates in Section 3.3 using the linear model with a density constraint.

Note that while the accretion disk model we adopt here is valid only for an accretion disk in steady-state, which may not be a valid assumption for a maser disk in reality because the timescale for such a disk to achieve steady state can be as long as a few  $\times 10^9$  years (e.g. Gammie, Narayan, and Blanford 1999), the consistent  $M_{\text{BH}}$  and  $M_{\text{D}}$  derived from the linear model and the Herrstein model suggests that our model fitting is not highly sensitive to the actual density distribution of the disk.

### 3.5. The Effect of Gas and Radiation Pressure on Maser Disks

One important assumption that has been made in the disk modeling discussed above is that the dynamical effect of gas and radiation pressure is negligible in comparison with gravity from the BH. This assumption can be tested by including the pressure terms in Equation (3) (Haworth et al. 2018) :

$$v_{\text{orb}} = \sqrt{\frac{GM_{\text{BH}}}{r} - \frac{f_{\text{rad}} r}{\rho} + \frac{r}{\rho} \frac{dP_{\text{gas}}}{dr}}, \quad (10)$$

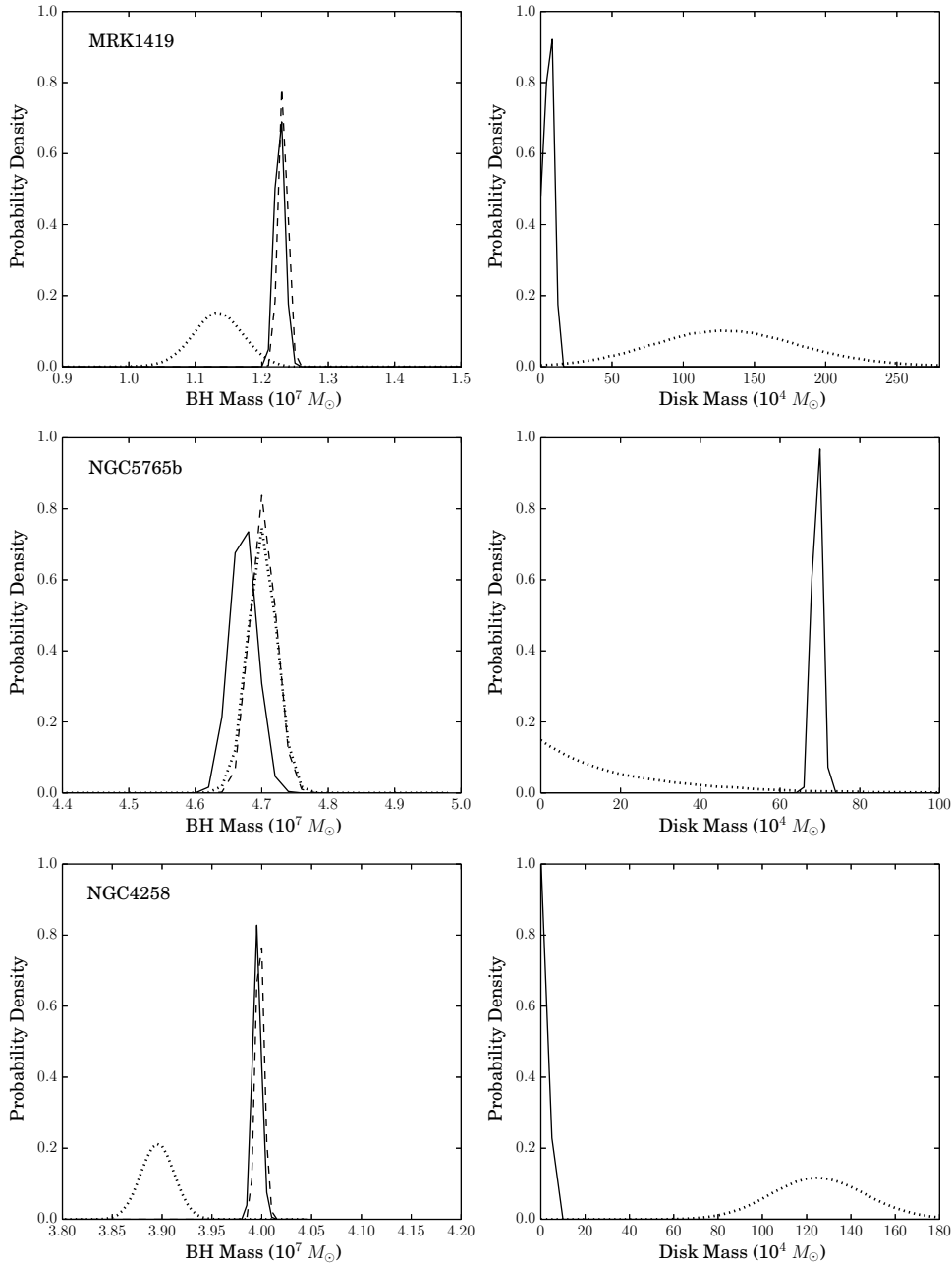


FIG. 3.— The posteriori probability distribution functions (PDF) of the black hole mass and disk mass from the 3-dimensional disk modelling based on the Huré model for the Keplerian maser disks in MRK 1419, NGC 5765b, and NGC 4258. The dashed lines shown in the left panels represent the PDFs of  $M_{\text{BH}}$  derived from the fiducial model in which the disk mass is assumed to be zero. The dotted and solid lines in the left and right panels show the fitting results from the linear model which either including (the solid line) or ignoring (the dotted line) the physical conditions for maser emission in the model fitting.

where  $f_{\text{rad}}$  is the radiation pressure force per unit volume,  $\rho$  is the local volume density, and  $P_{\text{gas}}$  is the thermal pressure of the gas in the maser disk. Assuming that the standard picture of maser excitation in an accretion disk (Neufeld, Maloney, Conger 1994; Neufeld & Maloney 1995) is correct, the mid-plane gas in a warped maser disk is directly illuminated by the AGN radiation obliquely which heat the gas to sufficient temperature for maser excitation. Assuming that the AGN radiation is isotropic and totally absorbed by the maser disk, we can

thus re-write the second term in equation (10) as

$$\frac{f_{\text{rad}} r}{\rho} = \frac{L_{\text{bol}}}{4\pi c r m_{\text{H}_2} n_{\text{H}_2}(r) H(r)} \sin(\alpha(r)), \quad (11)$$

where  $L_{\text{bol}}$  is the bolometric luminosity of the AGN,  $c$  is the speed of light, and  $\alpha(r)$  is the angle between the warped plane of the maser disk at radius  $r$  and the incident light ray that hits the disk plane. Since all maser disks discussed in this paper are only slightly warped, the angle  $\alpha$  is typically only a few degrees (e.g. Reid et al. 2013; Gao et al. 2016).

Assuming that the density distribution follows Equa-

TABLE 2  
RESULTS OF BAYESIAN DISK FITTING

| Galaxy Name | Model      | Masing Condition | $M_{\text{BH}}$<br>( $10^7 M_{\odot}$ ) | $\dot{M}$<br>( $10^{-4} M_{\odot} \text{ yr}^{-1}$ ) | $M_{\text{D}}$<br>( $10^7 M_{\odot}$ ) | $R_{\text{in}}$<br>(pc) | $R_{\text{out}}$<br>(pc) | $n_{\text{in}}$<br>( $10^9 \text{ cm}^{-3}$ ) | $n_{\text{out}}$<br>( $10^9 \text{ cm}^{-3}$ ) | $\chi^2_{\nu}$ |
|-------------|------------|------------------|---|--|--|-------------------------|--------------------------|---|--|----------------|
| UGC 3789    | Fiducial   | —                | $1.071^{+0.004}_{-0.004}$               | —  | —                                      | —                       | —                        | —   | —  | 0.642          |
| UGC 3789    | Linear     | No               | $1.065^{+0.007}_{-0.009}$               | —  | $0.010^{+0.014}_{-0.008}$              | 0.075                   | 0.203                    | $40^{+60}_{-33}$                              | $3.3^{+4.8}_{-2.7}$                            | 0.626          |
| UGC 3789    | Linear     | Yes              | $1.071^{+0.004}_{-0.004}$               | —  | $0.0013^{+0.0007}_{-0.0007}$           | 0.075                   | 0.203                    | $6^{+3}_{-3}$                                 | $0.5^{+0.3}_{-0.3}$                            | 0.697          |
| UGC 3789    | Herrnstein | No               | $1.068^{+0.005}_{-0.006}$               | $71^{+100}_{-53}$                                    | $0.007^{+0.001}_{-0.005}$              | 0.075                   | 0.203                    | $65^{+90}_{-48}$                              | $3.2^{+4.3}_{-2.4}$                            | 0.600          |
| UGC 3789    | Herrnstein | Yes              | $1.071^{+0.004}_{-0.004}$               | $7^{+4}_{-3}$  | $0.0007^{+0.0003}_{-0.0003}$           | 0.075                   | 0.203                    | $6^{+3}_{-3}$                                 | $0.3^{+0.1}_{-0.1}$                            | 0.595          |
| NGC 6323    | Fiducial   | —                | $0.992^{+0.007}_{-0.007}$               | —  | —                                      | —                       | —                        | —   | —  | 0.514          |
| NGC 6323    | Linear     | No               | $0.949^{+0.029}_{-0.039}$               | —  | $0.061^{+0.058}_{-0.041}$              | 0.144                   | 0.309                    | $31^{+29}_{-21}$                              | $4.5^{+3.9}_{-3.0}$                            | 0.513          |
| NGC 6323    | Linear     | Yes              | $0.984^{+0.008}_{-0.008}$               | —  | $0.011^{+0.06}_{-0.06}$                | 0.145                   | 0.306                    | $6^{+3}_{-3}$                                 | $0.8^{+0.5}_{-0.5}$                            | 0.502          |
| NGC 6323    | Herrnstein | No               | $0.976^{+0.013}_{-0.015}$               | $346^{+326}_{-228}$                                  | $0.034^{+0.032}_{-0.027}$              | 0.144                   | 0.309                    | $41^{+39}_{-27}$                              | $4.1^{+3.5}_{-2.7}$                            | 0.491          |
| NGC 6323    | Herrnstein | Yes              | $0.990^{+0.007}_{-0.007}$               | $48^{+31}_{-27}$                                     | $0.005^{+0.003}_{-0.003}$              | 0.145                   | 0.306                    | $6^{+3}_{-3}$                                 | $0.6^{+0.3}_{-0.3}$                            | 0.470          |
| NGC 6264    | Fiducial   | —                | $2.939^{+0.012}_{-0.010}$               | —  | —                                      | —                       | —                        | —   | —  | 0.778          |
| NGC 6264    | Linear     | No               | $2.716^{+0.047}_{-0.054}$               | —  | $0.262^{+0.071}_{-0.059}$              | 0.265                   | 0.483                    | $31^{+9}_{-7}$                                | $6.9^{+1.8}_{-1.5}$                            | 0.671          |
| NGC 6264    | Linear     | Yes              | $2.870^{+0.016}_{-0.013}$               | —  | $0.077^{+0.010}_{-0.015}$              | 0.268                   | 0.481                    | $9^{+1}_{-1}$                                 | $2.1^{+0.2}_{-0.4}$                            | 0.724          |
| NGC 6264    | Herrnstein | No               | $2.853^{+0.018}_{-0.018}$               | $749^{+212}_{-178}$                                  | $0.128^{+0.031}_{-0.227}$              | 0.264                   | 0.483                    | $41^{+10}_{-9}$                               | $6.7^{+1.6}_{-1.4}$                            | 0.664          |
| NGC 6264    | Herrnstein | Yes              | $2.916^{+0.012}_{-0.010}$               | $184^{+51}_{-51}$                                    | $0.030^{+0.004}_{-0.007}$              | 0.268                   | 0.481                    | $10^{+1}_{-1}$                                | $1.6^{+0.2}_{-0.4}$                            | 0.771          |
| Mrk 1419    | Fiducial   | —                | $1.237^{+0.007}_{-0.006}$               | —  | —                                      | —                       | —                        | —   | —  | 1.375          |
| Mrk 1419    | Linear     | No               | $1.139^{+0.037}_{-0.037}$               | —  | $0.133^{+0.054}_{-0.051}$              | 0.121                   | 0.310                    | $111^{+48}_{-44}$                             | $10.6^{+4.0}_{-3.9}$                           | 1.373          |
| Mrk 1419    | Linear     | Yes              | $1.232^{+0.007}_{-0.007}$               | —  | $0.008^{+0.004}_{-0.004}$              | 0.126                   | 0.307                    | $6^{+3}_{-3}$                                 | $0.6^{+0.3}_{-0.4}$                            | 1.362          |
| Mrk 1419    | Herrnstein | No               | $1.187^{+0.020}_{-0.020}$               | $637^{+285}_{-252}$                                  | $0.082^{+0.032}_{-0.032}$              | 0.121                   | 0.310                    | $152^{+69}_{-62}$                             | $9.0^{+3.4}_{-3.3}$                            | 1.064          |
| Mrk 1419    | Herrnstein | Yes              | $1.235^{+0.007}_{-0.006}$               | $36^{+18}_{-17}$                                     | $0.004^{+0.002}_{-0.002}$              | 0.126                   | 0.307                    | $8^{+3}_{-4}$                                 | $0.5^{+0.2}_{-0.3}$                            | 1.064          |
| NGC 5765b   | Fiducial   | —                | $4.712^{+0.018}_{-0.018}$               | —  | —                                      | —                       | —                        | —   | —  | 0.894          |
| NGC 5765b   | Linear     | No               | $4.711^{+0.021}_{-0.021}$               | —  | $0.013^{+0.024}_{-0.011}$              | 0.302                   | 1.252                    | $0.5^{+0.9}_{-0.4}$                           | $0.02^{+0.03}_{-0.01}$                         | 0.770          |
| NGC 5765b   | Linear     | Yes              | $4.682^{+0.019}_{-0.019}$               | —  | $0.070^{+0.001}_{-0.001}$              | 0.326                   | 1.236                    | $2.9^{+0.2}_{-0.1}$                           | $0.1^{+0.004}_{-0.002}$                        | 0.997          |
| NGC 5765b   | Herrnstein | No               | $4.713^{+0.020}_{-0.020}$               | $30^{+50}_{-23}$                                     | $0.020^{+0.033}_{-0.015}$              | 0.321                   | 1.233                    | $1.5^{+2.6}_{-1.2}$                           | $0.03^{+0.04}_{-0.02}$                         | 0.737          |
| NGC 5765b   | Herrnstein | Yes              | $4.663^{+0.019}_{-0.018}$               | $107^{+32}_{-24}$                                    | $0.068^{+0.017}_{-0.009}$              | 0.332                   | 1.204                    | $5.0^{+1.3}_{-0.7}$                           | $0.1^{+0.03}_{-0.01}$                          | 0.989          |
| NGC 4258    | Fiducial   | —                | $4.000^{+0.004}_{-0.004}$               | —  | —                                      | —                       | —                        | —   | —  | 0.555          |
| NGC 4258    | Linear     | No               | $3.898^{+0.017}_{-0.017}$               | —  | $0.128^{+0.022}_{-0.021}$              | 0.114                   | 0.301                    | $239^{+45}_{-41}$                             | $21.0^{+3.9}_{-3.6}$                           | 0.490          |
| NGC 4258    | Linear     | Yes              | $3.998^{+0.004}_{-0.004}$               | —  | $0.004^{+0.001}_{-0.002}$              | 0.115                   | 0.299                    | $7^{+2}_{-3}$                                 | $0.7^{+0.2}_{-0.3}$                            | 0.550          |
| NGC 4258    | Herrnstein | No               | $3.936^{+0.010}_{-0.010}$               | $380^{+84}_{-74}$                                    | $0.089^{+0.014}_{-0.013}$              | 0.113                   | 0.300                    | $362^{+64}_{-59}$                             | $19.5^{+3.3}_{-3.1}$                           | 0.498          |
| NGC 4258    | Herrnstein | Yes              | $4.000^{+0.004}_{-0.004}$               | $8^{+3}_{-3}$  | $0.002^{+0.001}_{-0.001}$              | 0.114                   | 0.299                    | $7^{+2}_{-3}$                                 | $0.4^{+0.1}_{-0.2}$                            | 0.566          |

NOTE. — Column (1): Name of the galaxy; column (2): the accretion disk model used for Bayesian fitting; column (3): whether the physical conditions for 22 GHz water maser emission were imposed in the fitting; column (4): the best-fit black hole mass; column (5): the best-fit mass accretion rate, normalized by  $\alpha$ , the Shakura-Sunyaev viscosity parameter (Shakura & Sunyaev 1973). Here, we set  $\alpha = 1$ ; column (6): the best-fit disk mass; columns (7) and (8): the inner and outer radii of the maser disk; column (9): columns (10) and (11): the number densities of molecular hydrogen at the inner and outer edges of the maser disk; column (12) the reduced  $\chi^2$  of the fit. Distances adopted in the Bayesian fitting for UGC 3789, NGC 6323, NGC 6264, MRK 1419, NGC 5765b, and NGC 4258 were 46.4, 106.7, 139.4, 72.2, 126.3, 7.6 Mpc, respectively.

tion (5) and that the temperature does not vary in the masing region of the disk, one can express the third term of Equation (10) as

$$\frac{r dP_{\text{gas}}}{\rho dr} = -\frac{5P}{2\rho} = -\frac{5kT}{2m_{\text{H}_2}}. \quad (12)$$

To see the effect of these two pressure terms on the dynamical mass measurement more clearly, it is helpful to re-express Equation (10) in the form of dynamical mass :

$$\mu \equiv \frac{rv_{\text{orb}}^2}{G} = M_{\text{BH}} - \Delta M_{\text{rad}} - \Delta M_{\text{gas}}, \quad (13)$$

where  $\Delta M_{\text{rad}}$  is defined as

$$\Delta M_{\text{rad}} = \frac{L_{\text{bol}}}{4\pi c G m_{\text{H}_2} n_{\text{H}_2}(r) H(r)} \sin(\alpha(r)), \quad (14)$$

and  $\Delta M_{\text{gas}}$  is defined as

$$\Delta M_{\text{gas}} = \frac{5kTr}{2Gm_{\text{H}_2}}. \quad (15)$$

Assuming that  $H(r)$  follows Equation (6), the BH mass is  $10^7 M_{\odot}$ , the gas temperature  $T$  is 700 K and  $\alpha$  is  $3^\circ$ , the inner radius of the maser disk is 0.2 pc, and the number density  $n_{\text{H}_2}(r)$  at the inner radius is  $10^{10} \text{ cm}^{-3}$ , we can re-express Equation (14) & (15) as

$$\Delta M_{\text{rad}} = 1095 \left( \frac{L_{\text{bol}}}{10^{44} \text{ erg s}^{-1}} \right) \left( \frac{r}{0.2 \text{ pc}} \right) M_{\odot}, \quad (16)$$

$$\Delta M_{\text{gas}} = 336 \left( \frac{T}{700 \text{ K}} \right) \left( \frac{r}{0.2 \text{ pc}} \right) M_{\odot}. \quad (17)$$

These equations show that the gas and radiation pressure can indeed introduce a negative slope in a PDM diagram, leading to negative disk mass. However, given that the

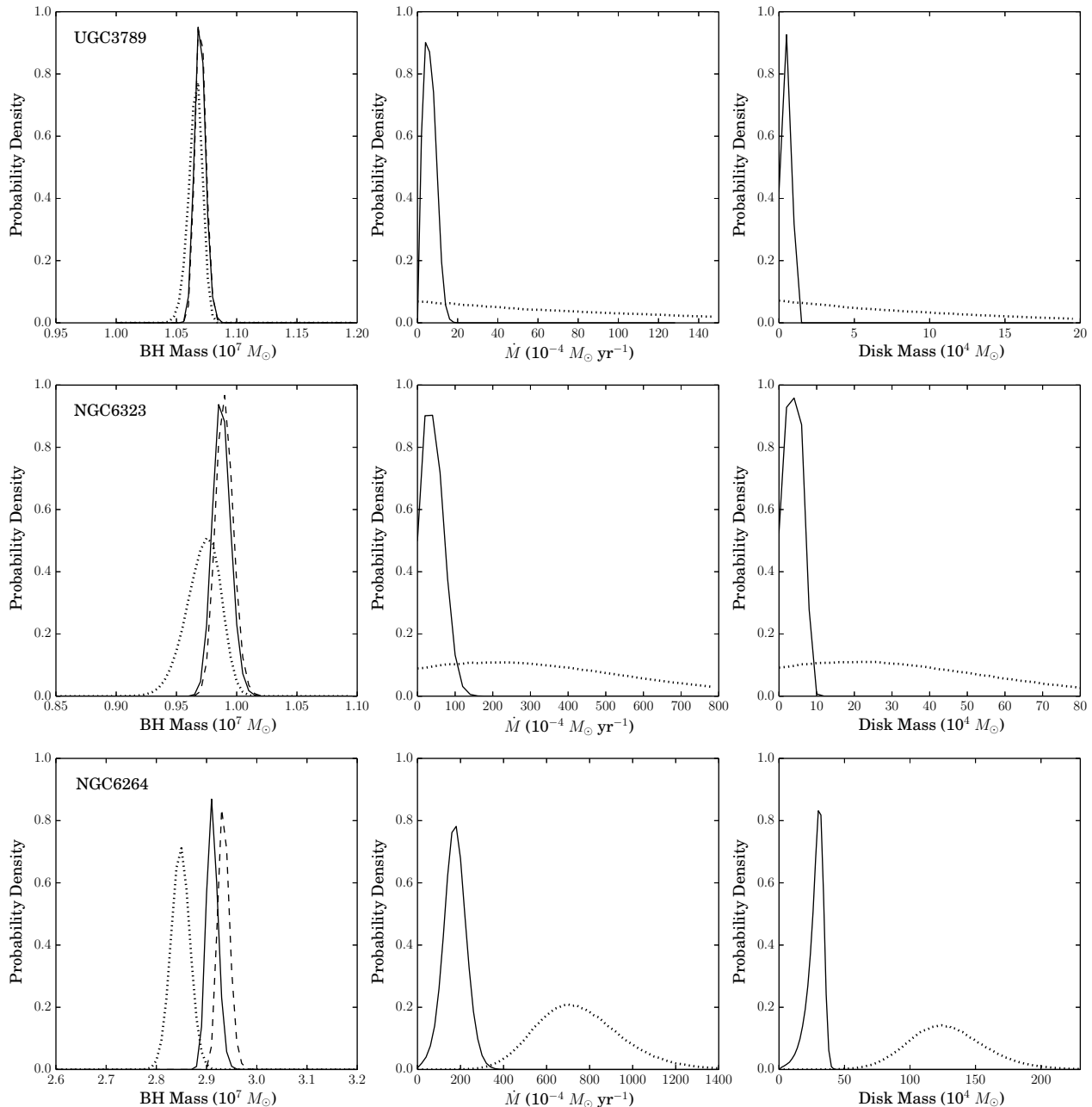


FIG. 4.— The posterior probability distribution functions (PDF) of the black hole masses, mass accretion rates, and disk masses from the 3-dimensional disk modelling based on the Herrnstein model for the Keplerian maser disks in UGC 3789, NGC 6323, and NGC 6264. The dashed lines shown in the left panels represent the PDFs of  $M_{\text{BH}}$  derived from the fiducial model in which the disk mass is assumed to be zero. The dotted and solid lines in the left and right panels show the fitting results from the Herrnstein model which either including (the solid line) or ignoring (the dotted line) the physical conditions for maser emission in the model fitting.

bolometric luminosities of AGN in the six maser galaxies range from  $\sim 1 \times 10^{42} - 6 \times 10^{44} \text{ erg s}^{-1}$  (Herrnstein et al. 2005; Greene et al. 2010; Gao et al. 2017), and the sizes of the maser disks are typically less than 1 pc, one can easily show that the pressure effects can only affect the dynamical mass estimates at the levels between 2 to 5 orders of magnitude lower than the black masses and cannot explain the scatter in the PDM diagram seen in Figure 1. From the above discussion, we can conclude that the thermal and radiation pressure are dynamically unimportant in comparison with the gravity of the BHs and can thus be ignored.

#### 4. DISCUSSION AND SUMMARY

The  $\text{H}_2\text{O}$  megamaser technique provides a unique way to determine the Hubble constant and BH mass with high accuracy, and systematic uncertainties in these parameters are thought to be small. The effectiveness of this method comes from the observation that the physics of the maser disk is relatively simple, clean, and well understood. There are only a few assumptions in the disk modeling:

- The masing gas follow circular orbits around the central BH of the disk.

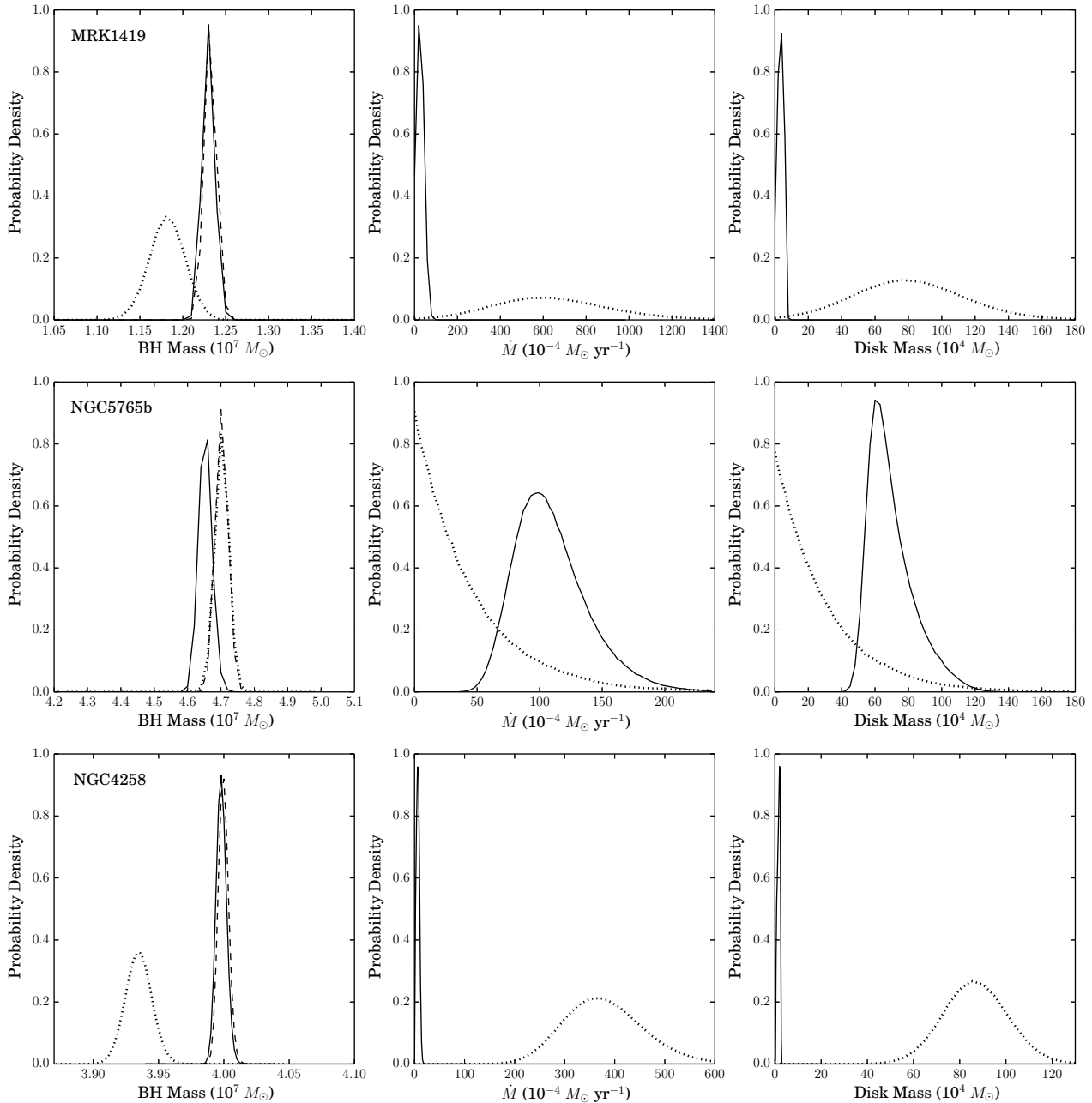


FIG. 5.— The posterior probability distribution functions (PDF) of the black hole masses, mass accretion rates, and disk masses from the 3-dimensional disk modelling based on the Herrnstein model for the Keplerian maser disks in UGC 3789, NGC 6323, and NGC 6264. The dashed lines shown in the left panels represent the PDFs of  $M_{\text{BH}}$  derived from the fiducial model in which the disk mass is assumed to be zero. The dotted and solid lines in the left and right panels show the PDFs for  $M_{\text{BH}}$  and  $M_{\text{D}}$  from the Huré model. The dotted and solid lines in the left and right panels show the fitting results from the Herrnstein model which either including (the solid line) or ignoring (the dotted line) the physical conditions for maser emission in the model fitting.

- The dynamics of the masing gas is dominated by the gravity of the BH and the effect of the self-gravity of the maser disk can be ignored. As a result, the gas follow Keplerian rotation *exactly* with negligible degree of deviation.
- The maser kinematics are minimally affected by non-gravitational forces such as radiation pressure (e.g. Maloney, Begelman, & Pringle 1996) or shocks from spiral density waves in the disk (e.g. Maoz & McKee 1998).

The first assumption can be directly tested by allowing orbital eccentricity ( $e$ ) to be a free parameter in the 3-dimensional modelling program. Based on results to date, there is no evidence for significant eccentricities (i.e.  $e > 0.1$ ), which could introduce significant systematics in parameter estimation (e.g. Reid et al. 2013; Humphreys et al. 2013). Therefore, this assumption has been well tested.

The existence of spiral density waves in maser disks was suggested by Maoz & McKee (1998), owing to some potential periodicities observed in the spatial distribu-

tion of high-velocity masers toward NGC 4258. Pesce et al. (2015) evaluated several sources and concluded that there is little evidence for spiral structure for most published Keplerian maser disks. This suggests that effects of the putative spiral density waves in maser disks on  $H_0$  determination is most likely to be negligible.

The only assumptions that have not been previously examined in some detail are the possible effects of radiation/gas pressure and the impact of self-gravity of maser disks on disk parameter estimation.

Ignoring self-gravity was expected to introduce negligible systematic errors ( $\lesssim 1\%$ ) in the modeling, as the masers often displayed near-perfect Keplerian motions. However, the work done by Huré et al. (2011) challenged this point of view. These authors suggested that disk masses in the maser galaxies NGC 4258 and UGC 3789 are a few times  $10^6 M_\odot$ , with the disk mass comparable to the BH mass in UGC 3789.

To understand why a Keplerian disk can have substantial disk mass, we re-examine the PDM diagram proposed by Huré et al. (2011). We show that while the linear disk model proposed by Huré et al. (2011) provides an easy and useful method to describe the self-gravity effect of the maser disk, the PDM diagram may not be an appropriate tool to infer BH mass and disk mass, because the maser data are projected on the sky and one must allow for deviations from the simplest geometry by modeling in 3-dimensions. Ignoring these issues can result in

uncertain disk masses that sometimes yield nonphysical (negative) disk masses.

Despite the possibility that negative disk masses inferred from PDM diagrams could result from gas and radiation pressure, our discussion in section 3.5 demonstrates that the pressure effects are dynamically unimportant compared to the gravity of the BHs, suggesting that negative slopes in PDM diagrams cannot be caused by the pressure effects for the maser systems discussed in this paper.

Our analysis, described in Section 3.2, show that a full 3-dimensional modeling, which allows for disk mass, yields small values. When we include physical constraints on density in the disk, in order to allow water maser emission, the disk mass estimates drop to very low levels, hence verifying an important assumption made in the megamaser technique for BH mass and  $H_0$  determination based on Keplerian maser disks.

We thank the anonymous referee for providing valuable suggestions for improving this paper. This publication is supported by Ministry of Science and Technology, R.O.C. under the project 104-2112-M-110-014-MY3. This research has made use of NASA's Astrophysics Data System Bibliographic Services, and the NASA/IPAC Extragalactic Database (NED) which is operated by the Jet Propulsion Laboratory, California Institute of Technology, under contract with the National Aeronautics and Space Administration.

## REFERENCES

- Bregman, M., Alexander, T. 2012, *ApJ*, 748, 63  
 Braatz, J. A., Reid, M. J., Humphreys, E. M. L., Henkel, C., Condon, J. J., & Lo, K. Y. 2010, *ApJ*, 718, 657  
 Caproni, A., Abraham, Z., Livio, M., Mosquera Cuesta, H. J. 2007, *MNRAS*, 379, 135  
 Ferrarese, L. & Merritt, D. 2000, *ApJ*, 539, 9  
 Gammie, C. F., Narayan, R., Blandford, R. 1999, *ApJ*, 516, 177  
 Gao, F.; Braatz, J. A.; Reid, M. J.; Lo, K. Y.; Condon, J. J.; Henkel, C.; Kuo, C. Y.; Impellizzeri, C. M. V.; Pesce, D. W.; Zhao, W. 2016, *ApJ*, 817, 128  
 Gao, F., Braatz, J. A., Reid, M. J., Condon, J. J., Greene, J. E., Henkel, C., Impellizzeri, C. M. V., Lo, K. Y., Kuo, C. Y., Pesce, D. W., Wagner, J., Zhao, W. 2017, *ApJ*, 834, 52  
 Gebhardt, K. et al. 2000, *ApJ*, 539, 13  
 Gray, M. D., Baudry, A., Richards, A. M. S., Humphreys, E. M. L., Sobolev, A. M.; Yates, J. A. 2016, *MNRAS*, 456, 347  
 Greene, J. E., Peng, C. Y., Kim, M., Kuo, C.-Y., Braatz, J. A., Impellizzeri, C. M. V., Condon, J. J., Lo, K. Y., Henkel, C., Reid, Mark J. 2010, *ApJ*, 721, 26  
 Greene, J. E., Seth, A., Kim, M., Läscher, R., Goulding, A., Gao, F., Braatz, J. A., Henkel, C., Condon, J., Lo, K. Y., Zhao, W. 2016, 826, 32  
 Greenhill, L. J., Booth, R. S., Ellingsen, S. P., Herrnstein, J. R., Jauncey, D. L., McCulloch, P. M., Moran, J. M., Norris, R. P., Reynolds, J. E., Tzioumis, A. K. 2003, *ApJ*, 590, 162  
 Gültekin, K. et al. 2009, *ApJ*, 698, 198  
 Herrnstein, J. R., Moran, J. M., Greenhill, L. J., Diamond, P. J., Inoue, M., Nakai, N., Miyoshi, M., Henkel, C., Riess, A. 1999, *Nature*, 400, 539  
 Herrnstein, J. R.; Moran, J. M.; Greenhill, L. J.; Trotter, Adam S. 2005, *ApJ*, 629, 719  
 Haworth, T. J., Booth, R. A., Homan, W., Decin, L., Clarke, C. J., Mohanty, S. 2018, *MNRAS*, 473, 317  
 Humphreys, E. M. L.; Reid, M. J.; Moran, J. M.; Greenhill, L. J.; Argon, A. L. 2013, *ApJ*, 775, 13  
 Huré, J.-M., Hersant, F., Carreau, C., Busset, J.-P. 2008, *A&A*, 490, 477  
 Huré, J.-M., Hersant, F.; Surville, C.; Nakai, N.; Jacq, T. 2011, *A&A*, 530, 145  
 Impellizzeri et al. in prep.  
 Kuo, C. Y.; Braatz, J. A.; Condon, J. J.; Impellizzeri, C. M. V.; Lo, K. Y.; Zaw, I.; Schenker, M.; Henkel, C.; Reid, M. J.; Greene, J. E. 2011, *ApJ*, 727, 20  
 Kuo, C. Y.; Braatz, J. A.; Reid, M. J.; Lo, K. Y.; Condon, J. J.; Impellizzeri, C. M. V.; Henkel, C. 2013, *ApJ*, 767, 155  
 Kuo, C. Y., Braatz, J. A., Lo, K. Y., Reid, M. J., Suyu, S., Pesce, D., Condon, J. J., Henkel, C., Impellizzeri, C. M. V. 2015, *ApJ*, 800, 26  
 Lodato, G., Bertin, G. 2003, *A&A*, 408, 1015  
 Maloney, P. R., Begelman, M. C., Pringle, J. E. 1996, *ApJ*, 472, 582  
 Martin, R. 2008, *MNRAS*, 387, 830  
 Maoz, E.; McKee, C. F. 1998, *ApJ*, 494, 218  
 Neufeld, D. A., Maloney, P. R. 1995, *ApJ*, 447, 17  
 Pesce, D. W.; Braatz, J. A.; Condon, J. J.; Gao, F.; Henkel, C.; Litzinger, E.; Lo, K. Y.; Reid, M. J. 2015, *ApJ*, 810, 65  
 Reid, M. J.; Braatz, J. A.; Condon, J. J.; Lo, K. Y.; Kuo, C. Y.; Impellizzeri, C. M. V.; Henkel, C. 2013, *ApJ*, 767, 154  
 Riess et al. 2016, *ApJ*, 826, 56  
 Ulubay-Siddiki, A., Gerhard, O., Arnaboldi, M. 2009, *MNRAS*, 398, 535